Meo Santolo*, Sorrentino Vincenzo

J. Electrical Systems 11-1 (2015): 102-116

Regular paper

Discrete-Time Integral Variable Structure Control of Grid-Connected PV Inverter

JES
Journal of Electrical Systems

In the paper a new discrete-time integral variable structure control of grid-connected PV inverter is proposed in order to maximize the input power given by PV arrays and at the same time for using the grid-inverter as a reactive power compensator. In the last years different variable structure controls (VSC) have been proposed in literature. In spite these algorithms have been implemented on digital hardware, they have been developed by means of a time-continuous formulation neglecting the effects of a microprocessor-based implementation. Such approach can cause an increasing amplitude chatter of the state trajectories which means instability. The proposed VSC is fully formulated in discrete-time, taking into account the effects introduced by a microprocessor-based implementation. Moreover it introduces respect to the classical formalization of the VSC an integral action that improve the performance of the controlled system. After a detailed formalization of the proposed control algorithm, several numerical and experimental results on a three-phase grid-connected inverter prototype are shown, proving the effectiveness of the control strategy. Thanks to the proposed control law the controlled system exhibits fast dynamic response, strong robustness for modelling error and good current harmonic rejection.

Keywords: Sliding mode control, grid-connected inverter, renewable energy, PV inverter

Article history: Received 24 September 2014, Received in revised form 20 January 2015, Accepted 15 February 2015

1. Introduction

The PV market has grown over the past decade at a remarkable rate and it is on the way to become in prospective a major source of power generation for the world [1]. At the same time the research on the topic has been more and more increasing. The literature largely focused on the discussion about power inverter topologies and their control [2]-[9] and successively about smart-inverters [10]-[12]. Traditionally, grid-inverters do not provide ancillary services to the grid. Instead, main targets of the smart inverter are to maximize PV array output power ensuring highest possible efficiency and some ancillary services like the reactive power and voltage control, loss compensation, scheduling and dispatch, load following, system protection and so on.

Among these services the control of reactive power is of relevant importance and it can be easily given locally by the inverter based on the requests transmitted in real time by the network operator. Frequently the power converter interface from the dc source to the grid consists of a current controlled voltage source inverter (VSI). Classic control of grid-connected VSI is usually based on grid-voltage or virtual-flux [13]-[15] oriented vector control schemes.

The scheme decomposes the ac currents into the synchronously rotating reference frame components. The power flow control is then achieved by regulating the decomposed converter currents. As current regulators are commonly used hysteresis, linear PI, predictive current control, state feedback current controller and so on [16]-[21]. The

* Corresponding author: S. Meo, Department of Electrical Engineering and Information Technology, “Federico II” University, Via Claudio 21, Naples, Italy, E-mail: santolo.meo@unina.it

hysteresis current control is the widely used because compared with other control algorithms, it has many advantages with simple realization solution, fast dynamic response, insensitive to load parameter and intrinsic protection versus short circuits. However with this technique the frequency of switches varies with the current therefore the design of filtering becomes difficult, the stress of power module increases and the energy loss of switches becomes high. Predictive current control strategies calculate the inverter voltages required to force the current to follow the reference current. This method can offer a more precise current control with minimum harmonic distortion, but it requires more computing resources and a good knowledge of system parameters. Digital control techniques such as state feedback control facilitate a constant switching frequency operation and guarantee high performance.

Nevertheless the state feedback control are susceptible to uncertainty in parameters and external disturbances acting on the plant. The necessity of state-observers and on-line parameter estimation increases the computational time requirement. A possible solution to these problems is to adopt a sliding mode based control approach. As it is known the sliding mode control is a kind of nonlinear control introduced for controlling variable structure systems which guarantees stability and robustness against parameter, line, and load uncertainties. Moreover the SM control is relatively easy to implement as compared to other types of non-linear controls and it is a control having a high degree of flexibility in its design choices. Therefore, during recent years, lots of sliding-mode control strategies have been implemented in three-phase grid-connected photovoltaic inverter [22]-[29]. However these papers neglect the effect of the microprocessor-based implementation, treating the system as if the control signals were available at every instant. Instead, in digital control power applications the control input is computed at discrete instants and applied to the system during the sampling interval. For this reason, inevitably, a nonideal sliding regime will appear. This quasi-sliding regime is inherently different by the quasi-sliding regime which may appear in continuous-time systems due to nonideal behavior of the analog components and can make the system unstable [30].

As it is already proved [31], discrete VSC's cannot be obtained from their continuous counterpart by means of simple equivalence. Indeed, this approach does not assure generally any convergence of the state trajectories onto the sliding manifold and may result in an increasing amplitude chatter of the state trajectories around the sliding manifold which means instability. Consequently, an adequate discrete-time formulation of sliding mode control must be done. In order to overcome all the cited problems, in the paper a new discrete-time integral sliding-mode (DISMC) control is proposed. The introduction of an integral action to the classical SMC has been adopted for overcoming the main drawback of the sliding mode control.

As it is known the sliding mode control exhibits stability and robustness against parameter, line, and load uncertainties only after the occurrence of the sliding mode on the sliding manifold. On the contrary the Integral sliding mode consents to overcome this problem, as results robustness of the system is always guaranteed, also during the reaching phase. In the paper the proposed control algorithm is fully developed in a rotating d,q reference frame synchronous with the angular frequency of the grid and it is applied to control a grid-connected PV inverter in order to maximize the electrical energy produced by PV arrays and at the same time for using the grid-inverter as a reactive power compensator.

An MPPT developed by the same Authors is adopted for tracking the maximum power point of the renewable source. After a detailed formalization of the proposed discrete-time ISMC some numerical and experimental results on a three-phase grid-connected inverter prototype are shown, proving the effectiveness of the control strategy. Thanks to the proposed control law the controlled system exhibits fast dynamic response, strong robustness to modeling error and uncertainties and good current harmonic rejection.

2. Description of the controlled system

The considered controlled system is shown in Fig. 1. Its main parts are the power plant and the controller block. The power plant is composed by the PV arrays, the capacitors bank, the current controlled three phase VSI inverter, the filter inductance, the three-phase step-up transformer and current and voltage sensors on the DC link and on the grid.

In the following the main components of the power plant will be depicted.

2.1. The PV Array Characterization

A full characterization of the PV output voltage (like function of the load request, of the irradiance and of the temperature) has been experimentally carried out. Then the experimental data have been interpolated with the well known following mathematical model of PV array:

$$V = \frac{Ak\theta}{q} ln\left(\frac{I - I_{ph} - I_{sat}}{I_{sat}}\right) - r_s I \tag{1}$$

PV array consists of N_s cells in series formed the panel and of N_p panels in parallel according to the rated power required. The output voltage and current can be given by the following equations:

$$V_{dc} = N_s\left(V - r_s I\right) \tag{2}$$

$$I_{dc} = N_p I \tag{3}$$

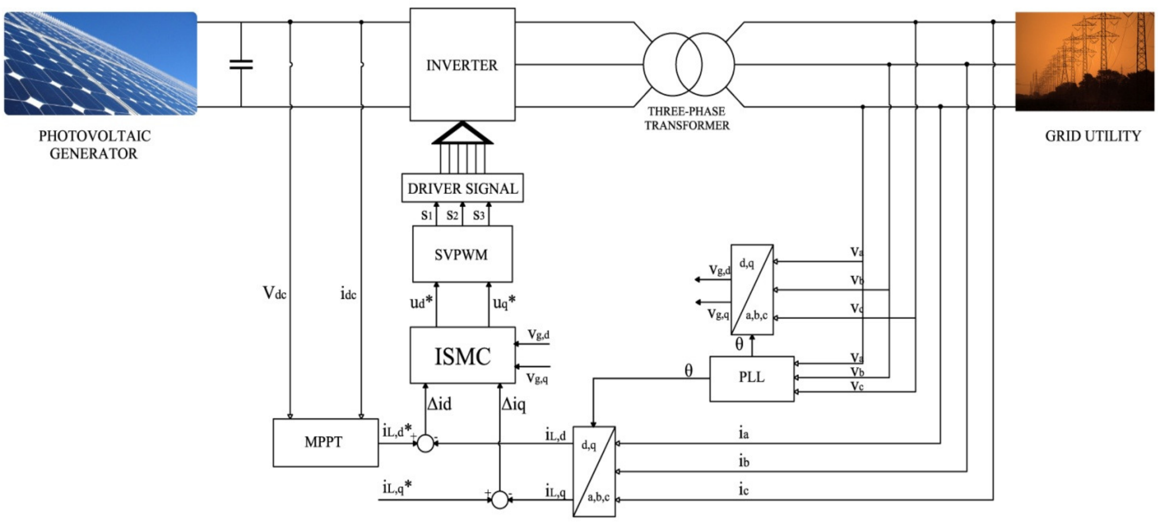

Fig. 1. Schema of the controlled system

2.2. Dynamic model of the voltage source inverter

Referring to the Fig. 2, the Kirchhoff voltage law applied to each phase yields (to simplify the analysis here, the transformer is neglected and only the filter inductance is considered):

$$V_{dc}s_k - L_f\frac{di_k}{dt} - (R_L + R_s)i_k - v_{g,k} - V_{NO} = 0 \tag{4}$$

where k= 1, 2, 3.

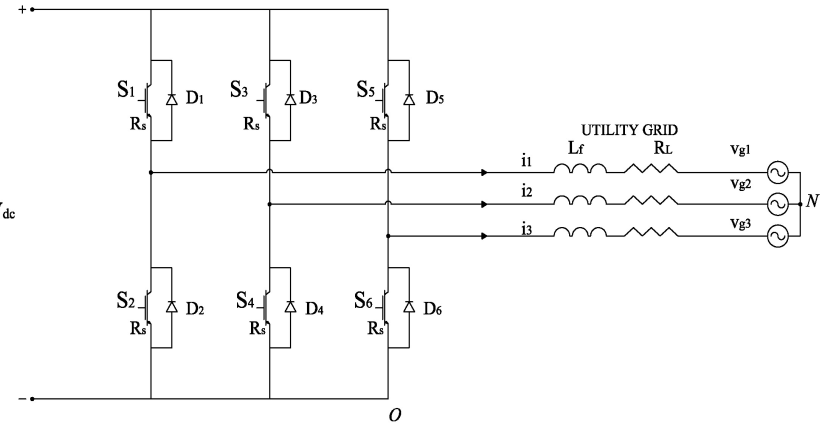

Fig. 2. Schema of the PVgrid-connected inverter

Having assumed that the system is symmetrical and balanced, the application of the currents Kirchhoff law at node N gives:

$$V_{NO} = -\frac{V_{dc}}{3}\sum_{n=1}^{3}s_n \tag{5}$$

Substituting the Eq. (5) in (4) it yields the following system of three differential equations:

$$L_f\frac{di_k}{dt} = V_{dc}\left(s_k - \frac{1}{3}\sum_{n=1}^{3}s_n\right) - Ri_k - v_{g,k} \tag{6}$$

where $R = (R_L + R_s)$

Now the following complex vectors (space vectors) shall be defined:

$$\mathbf{i} = \frac{2}{3}\sum_{k=1}^{3}i_k e^{j\frac{2\pi}{3}(k-1)},\quad \mathbf{u} = \frac{2}{3}V_{dc}\sum_{k=1}^{3}s_k e^{j\frac{2\pi}{3}(k-1)},\quad \mathbf{v}_g = \frac{2}{3}\sum_{k=1}^{3}v_{g,k}e^{j\frac{2\pi}{3}(k-1)} \qquad (7)\text{-}(8)\text{-}(9)$$

Multiplying both sides of Eq. (6) for the quantity $\frac{2}{3}e^{j\frac{2\pi}{3}(k-1)}$ and summing over k=1, 2, 3 one gets the following vectorial differential equation:

$$L_f \frac{d\mathbf{i}}{dt} = \mathbf{u} - R\mathbf{i} - \mathbf{v}_g \tag{10}$$

These space vectors are referred to a stationary reference frame. We can transform (8) from this stationary frame to a d-q synchronous frame rotating at the angular frequency ω of the grid voltages and having the d-axis aligned with the $\mathbf{v}_g$ space vector. In such reference frame by separating the real and imaginary parts, the Eq. (10) become:

$$\begin{cases} L_f \dfrac{di_d}{dt} = u_d - Ri_d - v_{g,d} + L_f \omega i_q \\ L_f \dfrac{di_q}{dt} = u_q - Ri_q - v_{g,q} - L_f \omega i_d \end{cases} \tag{11}$$

3. Control Design

The controller block is composed by the MPPT control algorithm, by the integral sliding mode controller and the grid interface (Fig. 1). In the following the main components of the control system will be depicted.

3.1. The adopted MPPT algorithm

The input to the control strategy are the d,q components id* and iq* of the desired grid currents. The adopted MPPT algorithm controls the maximization of the input power and gives the values of the reference current id* in the synchronous reference-frame. The used MPPT is an improved version of the classic P&O.

The improvement of the P&O algorithm has been obtained adjusting the perturbation width (ΔV) in function of the temperature. So, the dynamic response, when working conditions are far from the Maximum Power Point, can be improved without losing stability in the proximity of the Maximum.

It is well known that the voltage at which the power of a photovoltaic panel becomes maximum is almost independent on the solar irradiation but it is strongly dependent on the operating temperature. For this reason the same author has proposed to adapt the perturbation width according to the temperature variations. In order to achieve this aim, a temperature modelling of the photovoltaic arrays has been used. The MPPT algorithm will not be treated in the following. A detailed description of such algorithm can be found in [32]. The reference component iq* is computed according to the desired reactive power. For the calculation of these references the maximum apparent power of the three-phase inverter is also considered. When the PV system is not working at full power the three-phase inverter can also be working as reactive power compensator.

Obviously the grid injected reactive power is limited by the maximum apparent power of the inverter.

3.2. The grid interface

The grid interface provides the synchronization with the grid voltages by means of a classical Phase-Locked-Loop (PLL). The output of this block is necessary for the Park's transformation of the grid-voltages and of the grid-currents.

3.3. Integral Sliding Mode Control (ISMC)

The system of differential Equations (11) can be written in matrix form as follows (in balanced condition $v_{g,q}$ is null):

$$\begin{bmatrix} \dfrac{di_d}{dt} \\ \dfrac{di_q}{dt} \end{bmatrix} = \mathbf{A}\begin{bmatrix} i_d \\ i_q \end{bmatrix} + \mathbf{B}\begin{bmatrix} u_d \\ u_q \end{bmatrix} + \mathbf{c} \tag{12}$$

with:

$$\mathbf{A} = \begin{bmatrix} -\dfrac{R}{L_f} & \omega \\ -\omega & -\dfrac{R}{L_f} \end{bmatrix};\ \mathbf{B} = \begin{bmatrix} 1/L_f & 0 \\ 0 & 1/L_f \end{bmatrix};\ \mathbf{c} = \begin{bmatrix} \dfrac{-v_{g,d}}{L_f}, \dfrac{-v_{g,q}}{L_f} \end{bmatrix}^T \tag{13)-(14}$$

Indicating with:

$$x_1 = i_d(t) - i_d^*(t),\ x_2 = i_q(t) - i_q^*(t) \tag{15}$$

$$\mathbf{x} = [x_1\ x_2]^T \tag{16}$$

the system of differential Eqs. (12) can be re-writing with respect to the vector **x** giving:

$$\dot{\mathbf{x}} = \mathbf{A}\mathbf{x} + \mathbf{B}\mathbf{u} + \mathbf{D} \tag{17}$$

with:

$$\mathbf{D} = \mathbf{c} + \mathbf{A}\left[i_d^*, i_q^*\right]^T \tag{18}$$

The discrete-time formalization of the model (17), assuming zero-order hold on the control vector **u** can be given by:

$$\mathbf{x}_{k+1} = \mathbf{A}_d\mathbf{x}_k + \mathbf{B}_d\mathbf{u}_k + \mathbf{D}_d \tag{19}$$

where (Euler approximation):

$$\mathbf{A}_d = \mathbf{I} + \mathbf{A}T_s;\ \mathbf{B}_d = \mathbf{B}T_s;\ \mathbf{D}_d = \mathbf{D}T_s \tag{20}$$

and for the generic vector **a** is:

$$\mathbf{a}_k = \mathbf{a}(kT_s) \tag{21}$$

Firstly the objective of the SMC is to design a sliding manifold Σ so that the state trajectories of the system have the desired dynamic behavior. In particular the sliding manifold is generally defined as follows:

$$\Sigma = \left\{ \mathbf{x}_k : \boldsymbol{\sigma}_k = \boldsymbol{\sigma}\left(\mathbf{x}_k\right) = 0 \right\} \tag{22}$$

Considering the control vector $\mathbf{u} \in \Re^m$, the sliding manifold Σ represents the intersection of m switching planes $\boldsymbol{\sigma}_{k,i}$, where $\boldsymbol{\sigma}_{k,i} = \left\{ \mathbf{x}_k : \boldsymbol{\sigma}_i\left(\mathbf{x}_k\right) = 0 \right\}$, being $\boldsymbol{\sigma}_i$ the i-th row of the matrix $\boldsymbol{\sigma}_k$.

Now the problem is to find a switching vectorial function $\boldsymbol{\sigma}_k$ so that the motion of the dynamical system when confined on Σ is stable. Secondly, the problem is to find a variable structure control law so that, in finite time, the states are forced onto (sliding manifold reaching condition) and subsequently remain (convergence condition) on the sliding manifold Σ [33]. Usually in the classical DSMC the switching function $\boldsymbol{\sigma}_k$ is defined as:

$$\boldsymbol{\sigma}_k = \mathbf{K}\mathbf{x}_k \tag{23}$$

In our case as switching function we adopt the proportional-integral functions with the errors among the d,q components of the reference grid-currents and the actual ones. In other words let us define the switching function as follows:

$$\boldsymbol{\sigma}_k = \mathbf{K}\mathbf{x}_k + \mathbf{H}T_s \sum_{\rho=0}^{k-1} \mathbf{x}_\rho \tag{24}$$

where **K** and **H** are *mxm* matrices that will be chosen as depicted in the following.

The introduction of an integral action to the classical SMC has been adopted for overcoming the main drawback of the sliding mode control. As it is known the sliding mode control exhibit stability and robustness against parameter, line, and load uncertainties only after the occurrence of the sliding mode on the sliding manifold. On the contrary the integral sliding mode consents to overcome this problem.

Indeed with ISMC, the system trajectory always starts from the sliding surface.

Accordingly, the reaching phase is eliminated and robustness in the whole state space is obtained [33]- [34]. Motion in sliding mode implies that:

$$\boldsymbol{\sigma}_{k+1} = 0 \quad k = 0,1,2,3,... \tag{25}$$

Substituting (24) into the Eq. (25) yields:

$$\boldsymbol{\sigma}_{k+1} = \mathbf{K}\mathbf{x}_{k+1} + \mathbf{H}T_s \sum_{\rho=0}^{k} \mathbf{x}_k = \boldsymbol{\sigma}_k + \mathbf{K}\left(\mathbf{x}_{k+1} - \mathbf{x}_k\right) + \mathbf{H}T_s\mathbf{x}_k \tag{26}$$

and finally:

$$\mathbf{x}_{k+1} = \left(\mathbf{I} - \mathbf{K}^{-1}\mathbf{H}T_s\right)\mathbf{x}_k \tag{27}$$

Equation (27) describes the system dynamic on the switching manifold. As can be noted the convergence velocity is independent of the system parameters, depending only on the matrices **K** and **H**. Next step is to design the control law for the sliding-mode controller.

The control vector is structured as follows:

$$\mathbf{u}_k = \mathbf{u}_{eq,k} + \mathbf{u}_{s,k} \tag{28a}$$

Following the equivalent control method [33], we choice the so-called discrete-time equivalent control $\mathbf{u}_{eq,k}$ as the solution of the Eq. (25).

Substituting Eqs. (26) and (19) in the Eq. (25) and solving respect to $\mathbf{u}_k$ it yields:

$$\mathbf{u}_{eq,k} = -\left(\mathbf{KB}_d\right)^{-1}\left[\left(\mathbf{KA}_d + T_s\mathbf{H} - \mathbf{K}\right)\mathbf{x}_k + \mathbf{KD}_d + \boldsymbol{\sigma}_k\right] \tag{28b}$$

Ideally, $\mathbf{u}_{eq,k}$ is a solution to the discrete-time sliding mode control because it maintains the state on the sliding manifold at each sampling instant. In addition, it is not a switching type of control law; hence, no chattering phenomenon would occur if only $\mathbf{u}_{eq,k}$ is employed.

Thanks to the application of the control vector $\mathbf{u}_{eq,k}$ the state vector starting from the initial point $\mathbf{x}_0$ reaches theoretically in one sampling time the sliding manifold.

Unfortunately, such result in practice is not possible for two main problems: 1) parametric uncertainties and exogenous perturbations that influence the modelling giving poor robustness to the control and also because 2) $\mathbf{u}_{eq,k}$ may exceed the available control resources tending to the infinity if the initial state is far from Σ or if the sampling period is small. The switching control vector $\mathbf{u}_{s,k}$ is therefore necessary to complete the reachability condition and to reduce the reaching time giving robustness to the control, avoiding the first problem.

Such vector is generally chosen as follows:

$$\mathbf{u}_{s,k} = -\left(\mathbf{KB}_d\right)^{-1}\left[\mathbf{E}sign\left(\boldsymbol{\sigma}_k\right)\right] \tag{28c}$$

being: $sign\left(\boldsymbol{\sigma}_k\right) = \left[sign\left(\boldsymbol{\sigma}_k(1,1)\right), sign\left(\boldsymbol{\sigma}_k(2,1)\right)\right]^T$ (29)

(**E** is a constant matrix with all non-negatives elements).

Moreover it is necessary to take into account also the effective limits u_0 of the control (avoiding the second cited problem) imposing:

$$\begin{cases} \left\|\mathbf{u}_k\right\| \le u_0 \\ \left\|\left(\mathbf{KB}\right)^{-1}\right\| \cdot \left\|\left[\left(\mathbf{KA}_d + T_s\mathbf{H} - \mathbf{K}\right)\mathbf{x}_k + \mathbf{KD}_d\right]\right\| < u_0 \end{cases} \tag{30}$$

(being $\left\|\mathbf{u}_k\right\| = \left(\mathbf{u}_k^T\mathbf{u}_k\right)^{1/2}$) otherwise, the control resources are insufficient to stabilize the system.

For this reason the final variable structure control law will be the following:

$$\mathbf{u}_k = \begin{cases} \mathbf{u}_{eq,k} + \mathbf{u}_{s,k} & \text{for } \left\|\mathbf{u}_{eq,k} + \mathbf{u}_{s,k}\right\| \le u_0 \\ u_0 \dfrac{\mathbf{u}_k}{\left\|\mathbf{u}_k\right\|} & \text{for } \left\|\mathbf{u}_{eq,k} + \mathbf{u}_{s,k}\right\| > u_0 \end{cases} \tag{31}$$

To guarantee the global stability of the sliding-mode control system is equivalent to guarantee sliding manifold reaching condition and the convergence condition.

Many literatures have been developed to deal with the problem of designing stable sliding manifold for continuous-time systems; on the contrary, the literature dealing with the problem of designing stable sliding manifold for discrete-time SMC is not wide. Unfortunately, the sliding mode and reaching condition of the discrete VSC systems are different by those for continuous VSC systems. Generally, according to Lyapunov's theory, in the case of continuous-time systems, for example a sufficient condition so that the control system is stable and the system states can convergence to the sliding mode surface in the whole phase space is the verification of the following inequality:

$$\boldsymbol{\sigma}^T \dot{\boldsymbol{\sigma}} < 0 \tag{32}$$

A continuous counterpart of the inequality (26) by means of simple equivalence obtained substituting the time-derivative by the forward difference is the following:

$$\boldsymbol{\sigma}_k \left(\boldsymbol{\sigma}_{k+1} - \boldsymbol{\sigma}_k\right) < 0 \tag{33}$$

This condition, differently by the case of continous-time systems, is necessary but not sufficient for the existence of a discrete-time sliding motion [31].

Generally this condition does not assure any convergence of the state trajectories onto the sliding manifold and may result in an increasing amplitude chatter of the state trajectories around the sliding manifold which means instability [30]. A necessary and sufficient condition can be imposed assuring both sliding motion and convergence onto the sliding manifold. This condition may be stated as:

$$\left\|\boldsymbol{\sigma}_{k+1}\right\| < \left\|\boldsymbol{\sigma}_k\right\| \tag{34}$$

The proposed variable structure control law satisfies banally the condition (34) in the case that $\left\|\mathbf{u}_{eq,k}\right\| \le u_0$. To prove the condition (34) we will consider the case $\left\|\mathbf{u}_{eq,k}\right\| > u_0$. Substituting Eqs. (28) and (31) in the Eq. (26) and takes into account (30), it yields:

$$\boldsymbol{\sigma}_{k+1} = \begin{bmatrix} \left(\mathbf{KA}_d + T_s\mathbf{H} - \mathbf{K}\right)\mathbf{x}_k + \\ +\mathbf{KD}_d + \boldsymbol{\sigma}_k \end{bmatrix} \left(1 - \frac{u_0}{\left\|\mathbf{u}_k\right\|}\right) - \mathbf{E}sign\left(\boldsymbol{\sigma}_k\right)\frac{u_0}{\left\|\mathbf{u}_k\right\|} \tag{35}$$

thus:

$$\left\|\boldsymbol{\sigma}_{k+1}\right\| \le \left\|\boldsymbol{\sigma}_k\right\| + \left\|\left[\left(\mathbf{KA}_d + T_s\mathbf{H} - \mathbf{K}\right)\mathbf{x}_k + \mathbf{KD}_d\right]\right\| - \frac{u_0}{\left\|\left(\mathbf{KB}\right)^{-1}\right\|} \le \left\|\boldsymbol{\sigma}_k\right\| \tag{36}$$

Hence $\|\boldsymbol{\sigma}_{k+1}\|$ decreases monotonically and after a finite numbers of sampling times the states are forced onto and subsequently remain on the sliding manifold.

Therefore is proved that the proposed control law (31) satisfies the inequality (34) and guarantees the convergence and the global stability of the solution.

At end, in order to assure a fast convergence it is fundamental the choice of a suitable values in the matrices **K** and **H**.

In particular if $\boldsymbol{\sigma}_k \in \mathbb{R}^m$ $\mathbf{x}_k \in \mathbb{R}^n$, **K** and **H** are constant matrices of rank *m* and they are chosen such that [34]:

1) **K** satisfies the following conditions:
   1.1) ($\mathbf{KB}_d$) is an invertible the matrix;
   1.2) the $\left[\mathbf{A}_d - \mathbf{B}_d\left(\mathbf{KB}_d\right)^{-1}\mathbf{KA}_d\right]$ has m zero poles and *n-m* poles inside the unit disk in the complex z-plane (this property must be satisfied only if $n \neq m$. In our case only the property 1.1 must be considered);
2) **H** is chosen so that: $\mathbf{H} = -\mathbf{K}\left[\mathbf{A}_d - I - \mathbf{B}_d\mathbf{G}\right]$ where **G** is a matrix so that the pole of the matrix $\mathbf{A}_d$-$\mathbf{B}_d\mathbf{G}$ are distinct and within the unit circle.

4. Simulation results

In order to verify the performance of the proposed control strategy based on the ISMC approach, some simulations have been developed using MATLAB/Simulink. Discrete models were used with a simulation step time of 1 μs. The electric parameters of the tested system are listed in Table I.

The PV generator has been simulated as depicted in the section 2.1 and was connected to the grid-inverter block.

A space vector PWM with a sampling frequency of 20 kHz was used.

Fig. 3 shows the grid-voltage, the grid-current and the actual and reference currents i_d, i_d* and i_q, i_q*. The reference component i_d* is step-changed at 0.132 s from 6.2 A (corresponding to a active power of 3kW) to 3.1A (corresponding to a active power of 1.5 kW) during a time of 300 μs and then backed to 6.2 A at 0.1723 s during the same time of 300 μs, while the reference reactive power is contextually fixed to zero (i_q*=0). For representing on the same figure also the phase grid voltage and the grid current the zero of the reference components i_d* and i_q* have been translated to the value of -12 A on the ordinate axis. As can be noted the current is always in phase with the voltage and exhibits a very fast response.

Fig. 4 shows the grid-voltage, the grid-current and the actual and reference currents i_d, i_d* and i_q, i_q*. The reference component i_q* is step-changed at 0.132 s from 0 A to 3.1A (corresponding to a reactive power of 1.5 kVA) during a time of 300 μs and then backed to 0 A at 0.1723 s during the same time of 300 μs, while the reference active power is contextually fixed to 3.1A (corresponding to a active power of 1.5 kW).

For representing on the same figure also the phase grid voltage and the grid current the zero of the reference components i_d* and i_q* has been translated to the value of -12 A on the ordinate axis. As can be noted the current is initially in phase with the voltage then, in correspondence of the reference change rapidly presenting a phase change of 45°. In all the simulation the ripple on the current is very low.

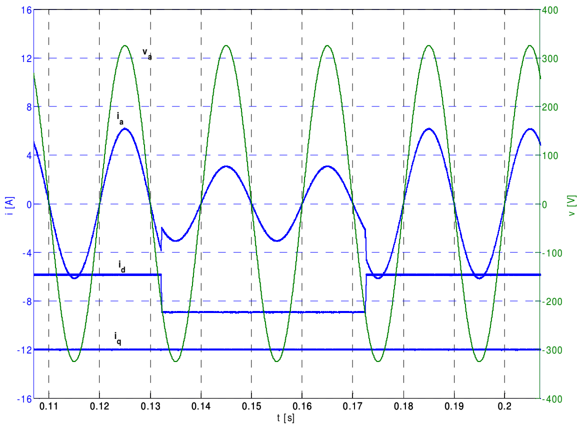

Fig. 3. Grid-voltage and grid-current, actual and reference currents i_d* and i_q* for a step change of i_d*

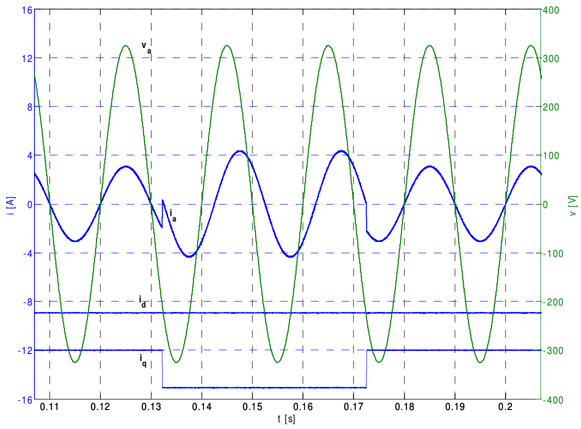

Fig. 4. Grid-voltage and grid-current, actual and reference currents i_d* and i_q* for a step change of i_q*

5. Experimental results

In order to validate the performances of the proposed control strategy an experimental prototype has been arranged. The Fig. 5 shows the experimental set-up that realizes the controlled system reported in Fig. 1 (grid inverter, transducers, transformer, evaluation board and so on). The control strategy has been developed in MATLAB/SIMULINK and implemented on DSP dSPACE1103 Motorola PowerPC 60K 333MHz.

The dSPACE1103 is a well known all-rounder in rapid control prototyping. A graphical user interface has been developed using the Control Desk software by dSPACE in order to control the converter and to monitor the electrical variables of the PV inverter. The main specifications of the experimental prototype are listed in the Table 1.

Table 1: Specifications of the experimetal prototype

Components		Rating values
PV generator (MITSUBISHI ELECTRIC PV) 10 strings connected in serie. Each string is composed of 3 modules in parallel (170 Wp per module).		5 kWp, 246 V, 21 A (@ STC)
PV module (PV-MF170EB4)		
Rating power (P_p)	170 Wp	
I_{sc} (short circuit current)	7.38 A	
V_{oc} (open circuit voltage)	30.6 V	
V_M (MPP voltage)	24.6 V	
I_M (MPP current)	6.93 A	
Temperature coefficient of V_{oc}	-0.346%/°C	
Temperature coefficient of I_{sc}	+0.057%/°C	
Temperature coefficient of P_p	-0.478%/°C	
IGBT/ Inverter Module	SEMIKRON 3xSKM 50 GB 123D	1200 V – 50 A (@ 25°C)
C_{PV}	input filter	DC Capacitor bank - Electrolytic 2x 2200µF/400V in series total equivalent capacitance 1100 µF/800 V
L_F, R_L, R_s	Grid side inductor and resistence	4 mH, 10 mΩ
GRID POWER TRANSFORMER	80 V / 400 V 3-phase 10kVA	

The Fig. 6 shows the Electrical characteristics of the adopted photovoltaic panel (Mitsubishi PV-MF170EB4). The Figs. 7 and 8 show the experimental response of the controlled system in the same operative conditions depicted in the Figures 3 and 4. Only the time scale is different and it can be deduced by the figures.

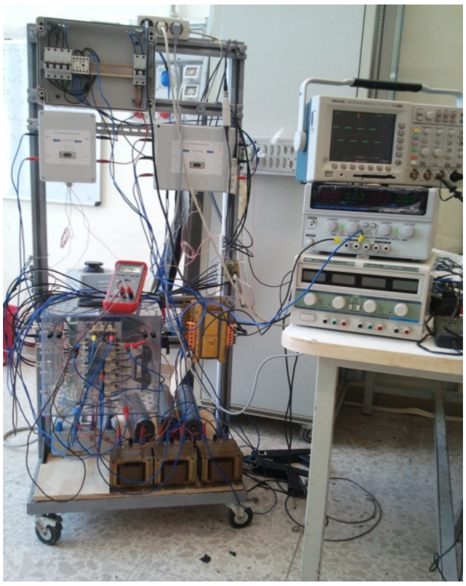

Fig. 5. Experimental setup

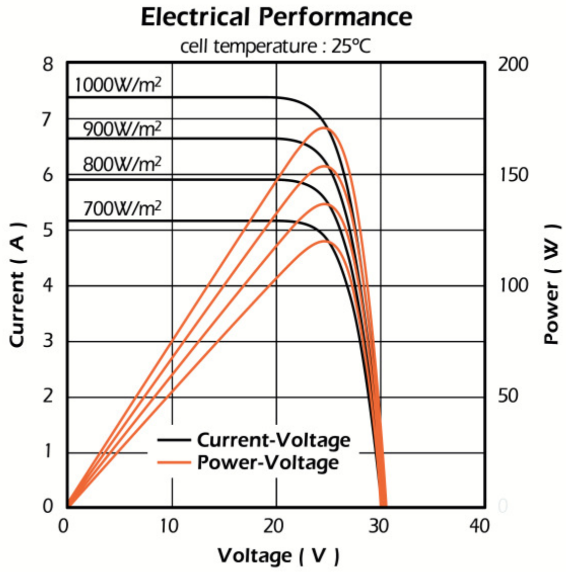

Fig. 6. Electrical characteristics of the adopted photovoltaic array for different irradiance conditions (Mitsubishi PV-MF170EB4)

The Figs. 7 and 8 show the experimental response of the controlled system in the same operative conditions depicted in the figures 3 and 4. Only the time scale is different and it can be deduced by the figures. As can be seen from the waveforms in figs. 7 and 8 compared with the figs. 3 and 4, the experimental results are in well accordance with the simulated ones. Fig. 9 illustrates the grid-current harmonic spectra. Each harmonic amplitude is expressed in percentage of the amplitude of the fundamental. The THD is 4.03 %. In all the considered operative conditions the current chattering on the references components of the grid currents has been always within ± 0.02 A. It is not shown in the figures only for space saving. In order to prove the robustness of the proposed control the electrical parameters of the system has been changed. The inductance LF has been reduced of 10 times respect to the values implemented in the control algorithm and RL has been incremented 10 times respect to the values implemented in the control algorithm. The Fig. 10 shows the simulation results obtained when the same operative conditions considered in fig. 3 are imposed to the controlled system. As can be noted even though the strong parametric modelling error the response of the system is very good.

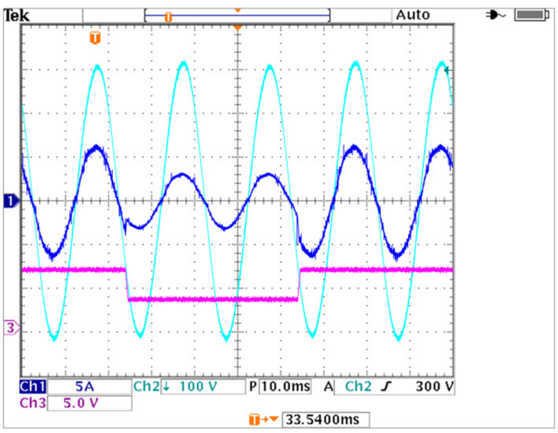

Fig. 7. Grid-voltage and grid-current, actual and reference currents i_d and i_q for a step change of i_d*

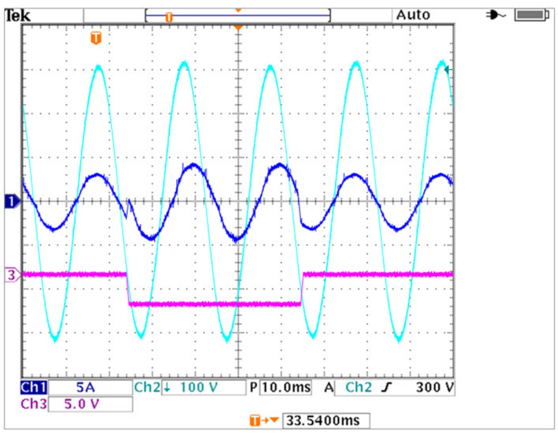

Fig. 8. Grid-voltage and grid-current, actual and reference currents i_d and i_q for a step change of i_q*.

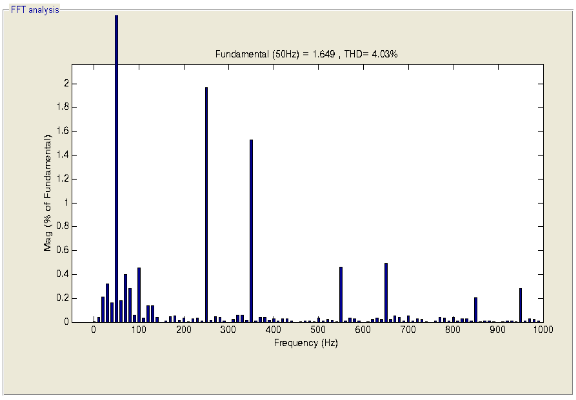

Fig. 9. Steady state grid-current harmonic spectra

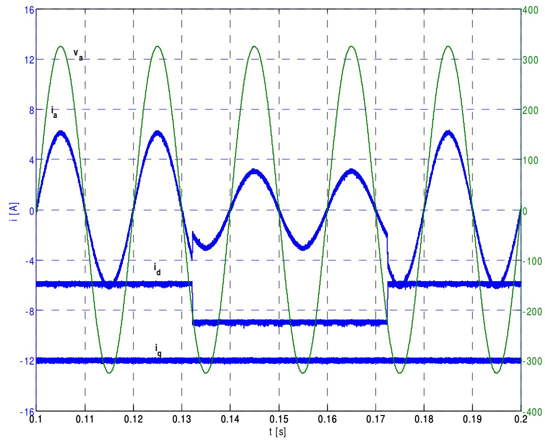

Fig 10. Grid-voltage and grid-current, actual and reference currents i_d* and i_q* for a step change of i_d* (with modelling error)

5. Conclusion

In the paper a new discrete-time integral variable structure control of grid-connected PV inverter is proposed in order to maximize the input power given by PV arrays and at the same time for using the grid-inverter as a reactive power compensator. The proposed VSC is fully formulated in discrete-time, taking into account the effects introduced by a microprocessor-based implementation and it introduces respect to the classical formalization of the VSC an integral action that improve the performance of the controlled system.

Thanks to the proposed control law the controlled system exhibits fast dynamic response, strong robustness for modelling error and good current harmonic rejection.

References

[1] Gaëtan Masson, Sinead Orlandi, Manoël Rekinger, Global Market Outlook for Photovoltaics 2014-2018, *European photovoltaic industry association (EPIA)*, June 2014.

[2] Y. Yang, P. Enjeti, F. Blaabjerg, and H. Wang, Suggested grid code modifications to ensure wide-scale adoption of photovoltaic energy in distributed power generation systems, in 2013 *IEEE Industry Applications Society Annual Meeting*, 2013, pp. 1 –8.

[3] L. Hassaine, E. OLias, J. Quintero, and V. Salas, Overview of power inverter topologies and control structures for grid connected photovoltaic systems, *Renewable and Sustainable Energy Reviews*, vol. 30, pp. 796

[4] Liu, L., Li, H., Xue, Y., Liu, W., Decoupled Active and Reactive Power Control for Large-Scale Grid-Connected Photovoltaic Systems Using Cascaded Modular Multilevel Converters, Power Electronics, *IEEE Transactions* on, Volume 30, Issue 1, 2015 , Page(s): 176-187

[5] Karuppusamy, A. M. Natarajan, Neuro Fuzzy Controller for Grid Connected Photovoltaic System with Multilevel Inverter, (2013) *International Review on Modelling and Simulations (IREMOS)*, 6 (3), pp. 693-705.

[6] M. Valan Rajkumar, P. S. Manoharan, Harmonic Reduction of Fuzzy PI Controller Based Three-Phase Seven-Level DCMLI with SVPWM for Grid Connected Photovoltaic System, (2013) *International Review on Modelling and Simulations (IREMOS)*, 6 (3), pp. 684-692.

[7] Rihab Mahjoub Essefi, Mansour Souissi, Hsan Hadj Abdallah, Current Control Strategy for Grid Connected Photovoltaic Inverter via LCL Filter, (2013) *International Review on Modelling and Simulations (IREMOS)*, 6 (5), pp. 1426-1434.

[8] Alessandro Burgio, Rosario Carbone, Rosario Morello, Anna Pinnarelli, Grid-Connected PV-Plants Based on a Distributed Energy-Storage System and a Multilevel Inverter, (2013) *International Review of Electrical Engineering (IREE)*, 8 (4), pp. 1267-1278.

[9] A. Damiano, G. Gatto, I. Marongiu, S. Meo, A. Perfetto, A. Serpi, Single-Stage Grid Connected PV Inverter with Active and Reactive Power Flow Control via PSO-PR Based Current Controlled SVPWM, (2012) *International Review of Electrical Engineering (IREE)*, 7 (4), pp. 4647-4654.

[10] Fernao Pires, V. , Martins, J. F. , Silva, J., F., A control structure for a photovoltaic supply system with power compensation characteristics suitable for smart grid topologies, Compatibility and Power Electronics (CPE), 2013 *8th International Conference on, Year: 2013* , Page(s): 40-45.
[11] Yang Han, Passivity-Based Control Scheme for the Modular Multilevel Cascaded Converter (MMCC) as the HVDC-PLUS for Smart Grid Applications, (2013) *International Review of Electrical Engineering (IREE)*, 8 (2), pp. 558-567.
[12] M. Hashmi, S. Hänninen, Kari Mäki Developing Smart Grid Concepts, Architectures and Technological Demonstrations Worldwide - A Literature Survey, (2013) *International Review of Electrical Engineering (IREE)*, 8 (1), pp. 236-252.
[13] M. P. Kazmierkowski, L. Malesani, Current control techniques for three-phase voltage-source PWMconverters: A survey, *IEEE Trans. Ind. Electron*., vol. 45, no. 5, pp. 691–703, Oct. 1998.
[14] Jiefeng Hu, Jianguo Zhu, Dorrell, D.G., Guerrero, J. M., Virtual Flux Droop Method, A New Control Strategy of Inverters in Microgrids, Power Electronics, *IEEE Transactions on*, Year: 2014, Volume 29, Issue 9, Page(s): 4704- 4711.
[15] Bo Fan, Jiexin Pu, Gang Liu, A Novel Study of Direct Power Control of Three-Phase Voltage Source PWM Rectifier Based on Virtual Flux, (2013) *International Review of Electrical Engineering (IREE),* 8 (1), pp. 60-64.
[16] Chen Xiaoju, Zhang Hang, Zhao Jianrong, A new Improvement Strategy based on hysteresis space vector control of Grid-connected inverter, Advanced Power System Automation and Protection (APAP), *2011 International Conference on* , vol.2, no., pp.1613-1617, 16-20 Oct. 2011.
[17] Bo Yang, Jiande Wu, Xiaodong Lu, Xiangning He, An improved DSP-based control strategy with predictive current control and fuzzy voltage control for grid-connected voltage source inverters, Industrial Electronics, 2008. *IECON 2008. 34th Annual Conference of IEEE* , vol., no., pp.2296-2300, 10-13 Nov. 2008.
[18] Xiang Hao, Tao Liu, Xu Yang, Lang Huang, A discrete-time integral sliding-mode controller with nonlinearity compensation for three-phase grid-connected photovoltaic inverter, *Power Electronics and Motion Control Conference (IPEMC),* 2012 7th International , vol.2, no., pp.831-835, 2-5 June 2012.
[19] Zare, F., Ledwich, G., A New Hysteresis Current Control for Three-phase Inverters Based on Adjacent Voltage Vectors and Time Error, *Power Electronics Specialists Conference*, 2007. PESC 2007. *IEEE*, vol., no., pp.431-436, 17-21 June 2007.
[20] Ayman Blorfan, Guy Sturtzer, Damien Flieller, Patrice Wira, Jean Mercklé, An Adaptive Control Algorithm for Maximum Power Point Tracking for Photovoltaic Energy Conversion Systems - A Comparative Study, (2014) *International Review of Electrical Engineering (IREE)*, 9 (3), pp. 559-565.
[21] Tarik Jarou, El Kachani Abderrahmane, El Haj Nabil, Niaaniaa Abdelhamid, New Control Based on Estimated State Feedback of the Shunt Active Filter to Compensate for the Disturbing Currents in the Electric Power, (2014) *International Review on Modelling and Simulations (IREMOS)*, 7 (3), pp. 457-465.
[22] Jiabing Hu, Lei Shang, Yikang He, Zhu, Z.Q., Direct Active and Reactive Power Regulation of Grid-Connected DC/AC Converters Using Sliding Mode Control Approach, Power Electronics, IEEE Transactions on, Volume 26, Issue 1, Publication Year: 2011, Page(s): 210 - 222.
[23] L. Shanmukha Rao, N. Venkata Ramana, Design of Robust Controller for Load Frequency Control in Deregulated Hydro-Thermal System Using Sliding Mode Controlled Strategies, (2013) *International Review on Modelling and Simulations (IREMOS)*, 6 (3), pp. 893-902.
[24] A. El-Jouni, M. Guisser, M. Salhi, A Sliding Mode Optimization of a Photovoltaic Pumping System, (2014) *International Review on Modelling and Simulations (IREMOS)*, 7 (3), pp. 466-473.
[25] M. Guisser, A. EL-Jouni, EL. H. Abdelmounim, Robust Sliding Mode MPPT Controller Based on High Gain Observer of a Photovoltaic Water Pumping System, (2014) *International Review of Automatic Control (IREACO)*, 7 (2), pp. 225-232.
[26] T. Anil Kumar, N. Venkata Ramana, Design of Sliding Mode Observer Based Optimal Controller for Load Frequency Control in Multi Area Deregulated Thermal System Connected with HVDC Link, (2013) *International Review on Modelling and Simulations (IREMOS)*, 6 (2), pp. 543-553.
[27] Abd Elwahed Touati, A. Abouloifa, E. Abd Elmounim, M. Aboulfatah, R. Majdoul, A. Moutabir, Modeling and Control of a Three Phase DC-AC Converter Connected to the Network for a Wind Power System Equipped with a DFIG, (2014) *International Review on Modelling and Simulations (IREMOS)*, 7 (2), pp. 231-237.
[28] Mohamed El Hachemi Benbouzid, Brice Beltran, Yassine Amirat, Sylvie Breton, Sensorless Control of Doubly-Fed Induction Generator-Based Wind Turbines Using a High-Order Sliding Mode Observer, (2014) *International Review of Electrical Engineering (IREE)*, 9 (1), pp. 49-55.
[29] Long Bo, Ji Hyoung Ryu, Young Won Jang, Kil To Chong, Sliding Mode Control of Energy Recovery Transformer-Less Power Accumulator Battery Pack Testing System, (2013) *International Review of Electrical Engineering (IREE)*, 8 (2), pp. 539-549.
[30] S. Z. Sarpturk, Y. Istefanopulos, O. Kaynak, On the stability of discrete-time sliding mode control systems, *IEEE Trans. Automat. Contr*., vol. 32, no. 10, pp. 93G932, 1987.
[31] D. Milosavljevic, General conditions for the existence of a quasi-sliging mode on the switching hyperplane in discrete variable structure system, *Automat. Remote Contr*., vol. 46, pp. 307-314, 1985.

[32] F. Esposito, V. Isastia, S. Meo, L. Piegari, An Improved Perturbe and Observe Algorithm for Tracking Maximum Power Points of Photovoltaic Power Systems, (2008) *International Review on Modelling and Simulations (IREMOS)*, 0 (0), pp. 10-16.

[33] Vadim Utkin, Juergen Guldner, Ma Shijun, Sliding mode control in electromechanical systems, *Taylor & Francis*, 1999.

[34] K. Abidi, J. X. Xu, and Y. Xinghuo, On the discrete-time integral sliding mode control, *IEEE Trans. Autom. Control*, vol. 52, no. 4, pp. 709–715, Apr. 2007.